Influence of the curing stress effect on the stiffness degradation curve of a silt stabilized with lime and cement

Lucile Pigeot, Nathalie Dufour, Hélène Calissano, Fabienne Dermenonville, Anthony Soive

Influence of the curing stress effect on the stiffness degradation curve of a silt stabilized with lime and cement.

Lucile Pigeot[A,B], Nathalie Dufour[B], Hélène Calissano[B], Fabienne Dermenonville[c], Anthony Soive[D]

[A] GeM, Ecole Centrale de Nantes, Nantes, France
[B] GeoCoD, Cerema, Aix-en-Provence, France
[C] Egis Structures et environnement, Seyssins, France
[D] Cerema, Aix-en-Provence, France
Corresponding author's E-mail: nathalie.dufour@cerema.fr

Abstract

This study investigated the shear modulus degradation curves of reconstituted stabilized soil specimens and their evolution during curing up to 270 days. An experimental protocol is proposed to get as close as possible to the *in situ* curing conditions of a chemically (lime and hydraulic binder) and mechanically (compaction) improved soil placed in a high-rise geotechnical structure. Innovative solutions now make it possible to build high embankments (> 10 m) in stabilized soil. In the laboratory, a silty soil stabilized with 1% lime and 5% hydraulic binder, which is a classic treatment for linear projects, was cured with a pressure of 300 and 500 kPa, corresponding to a depth in the embankment of 15 and 25 m. These structures are expected to have high mechanical performance and must be able to withstand very small deformations (earthquakes, traffic loads). Experimental campaigns are performed in laboratory using torsion tests with a resonant column apparatus (RCA) to obtain the shear modulus G as a function of distortion. A comparison was made between normalized curing conditions (temperature of 20°C and atmospheric pressure) and curing with confining pressure (temperature of 20°C and 300 or 500 kPa pressure). For this aim, 74 torsional RCA tests were conducted on 16 compacted soil specimens. These showed that the curing pressure, applied just after compaction, brings the expected properties more quickly and confers superior properties of around 15% in the long term. A power law was proposed to estimate the Gmax of a stabilized silt specimen as a function of time, based on the Gmax measured during the first two days of curing. This empirical law gives the Gmax over the long term (270 days) for curing with or without confining pressure. Pioneering a combined curing-testing RCA approach, this study elucidates the short and long-term behavior of stabilized silts under realistic curing conditions.

Keywords

Stabilized soil - Lime/Cement - Resonant column test – Shear Modulus degradation curves – Curing stress

1. Introduction

Economic and environmental imperatives are now prompting project owners to optimize the volumes of excavation/backfill by using *in situ* materials for earthworks. When these soils don't have the required mechanical performance, chemical and mechanical improvement solutions are used. In current linear projects (railway lines, roads and canals), soils are first stabilized with lime to improve their workability, then stabilized with hydraulic binder and compacted, which will give them greater rigidity, cohesion and strength. In order to reduce the carbon impact of these projects, the binders used are increasingly composed of Portland cement, combined with a low-carbon substitute (blast furnace slag, fly ash, etc.). Typical dosages for these projects are 1% lime and 4 or 5% hydraulic binder. Growing knowledge of these materials and their durability has encouraged their use in innovative solutions for geotechnical structures such as high embankments (> 10m).

To ensure that stabilized soils achieve the expected mechanical properties after chemical treatment and compaction, laboratory tests are carried out after different curing periods on reconstituted specimens or on specimens cored on experimental embankment (Bell, 1996; Makki-Szymkiewicz et al., 2015; Sariosseiri & Muhunthan, 2009; Wild et al., 1998). Curing period corresponds to the time required for the anhydrous phases contained in the lime and the cement to react with moist soil and form hydrated phases. Soils mechanical properties (strength, modulus) and intrinsic characteristics (permeability, void index) over time are controlled by laboratory tests on these specimens. These tests are executed to be as close as possible to the conditions in which the soil was in the field (state of stress, saturation and draining condition).

Previous authors have noticed a difference in mechanical properties between cemented materials collected on site and the same materials prepared in the laboratory (Consoli et al., 2000; Dalla Rosa et al., 2008). By applying, during curing time, stresses to the laboratory-cemented soils similar to those

present *in situ*, these authors noted that they approximate the mechanical properties of the cored materials. They define "curing stress" (CS) as the stresses applied to the specimen during its curing time. These initial observations were made on naturally or artificially-cemented sands by using an œdometric ring to study K0 (the coefficient of earth pressure at rest) (Zhu et al., 1995), then triaxial tests (Consoli et al., 2000; Filipe Veloso Marques et al., 2019; Taher et al., 2011) or UCS (Uniaxial Compressive Strength) tests (Liu & Starcher, 2013; Suzuki et al., 2014). These phenomena have also been observed on cement paste backfill (CPB) since the 1980s and on Deep Soil Mixing columns. The CPB method consists of forming tailings fills with 4%-10% cement addition in layers that are progressively buried (Chen et al., 2021; Cui & Fall, 2016; Fahey et al., 2011; Zhao et al., 2021). Soil mixing consists of creating rigid columns up to 50m depth by mixing soil with hydraulic binders (up to 30%) (Åhnberg, 2007; He et al., 2020; Yaghoubi et al., 2020; Zhang et al., 2017). The common point of these methods is that the mechanical properties measured on specimens reconstituted in the laboratory tend to be underestimated compared to those cored at great depth.

Hence, to reduce the disparity between the cemented materials properties measured in the laboratory and *in situ* cored specimens, it is necessary to recouple the hydration period and the confinement of the specimens undergoing long curing times. This means keeping the soil, during hydration, under confining pressure until its mechanical behavior is assessed by a geotechnical test.

A resonant column apparatus (RCA) in torsion mode was used to investigate the impact of the curing stress on the hydration kinetic of lime and binder- stabilized silty soil from a mechanical point of view (Chae et al., 1981; Chepkoit & Aggour, 1996; Chiang & Chae, 1972; Lang et al., 2020; Tsai & Ni, 2011). This apparatus had a double utility in our study. On one hand, the RCA test is considered as a nondestructive test (ASTM, 2021) that can be used on intact or reshaped specimens. This allows the soil specimen to be maintained in the confining cell, measurements to be taken at regular intervals, and provides the evolution of the shear modulus as a function of time on the same specimen. Consequently, the hydration evolution can be followed without modified curing conditions (temperature or pressure). On the other hand, it allowed us to capture soil behavior in small deformations (10^{e-7}-10^{e-4}), the dynamic

properties of stabilized soils required to anticipate their response under dynamic loading linked to earthquakes, traffic loads, and construction loads.

The materials used in the study are a silty soil to which 1% lime and 5% hydraulic binder by weight of material were added. This is a standard mix for linear infrastructure in France. The objective was to highlight the difference in shear modulus degradation curves for this stabilized soil with two curing conditions: one curing at atmospheric pressure (up to 270 days) and the other with isotropic curing stresses (300 kPa or 500 kPa) applied throughout the curing process (up to 28 and 70 days). These stresses correspond to backfill depths of around 15 and 26 m. After defined cure times, tests were performed on normalized specimens at two different isotropic testing pressures: 300 kPa or 500 kPa. At each testing pressure, tests were also carried out on compacted and untreated silt specimens. Finally, a law for predicting the shear modulus at very low strain (Gmax) as a function of curing time was proposed. It predicts Gmax for both curing conditions up to 270 days.

2. Materials and specimen preparation

2.1 Silty soil

The soil used in the study was a silt that comes from the North of France. It was extracted with an excavator and stored in bags. In the laboratory, it was sieved to 0.2 mm and passed through a riffle box for dividing soil aggregates into representative specimen increment for testing. The particle size analysis performed by laser diffraction showed that for the sieved soil, 80% of the grains were smaller than 0.008 mm and that the maximum grain diameter Dmax was equal to 0.1346 mm (ISO, 2020). The particle size curve (Figure 1) indicates a composition equivalent to 81% silt, 11% clay and 8% sand. The mineralogical composition was analyzed by X-ray diffraction (XRD): the silt was mostly composed of quartz, carbonate phases (calcite and dolomite), silicates (muscovite, microcline and clinochlore) feldspars (albite), clay minerals (kaolinite) and hematite. As summarized in Table 1, the soil was low clayey and had a low Plasticy Index (PI). This allows it to be classified according to the Unified Soil Classification System (USCS) as ML (silt with a low liquid limit) (ASTM, 2020). These characteristics

were similar to several silty soils from northern France (Das et al., 2022; Lemaire et al., 2013; Makki-Szymkiewicz et al., 2015).

Table 1: Geotechnical properties of silt used in the study.

Properties	Values
Methylene blue value VBS [g/100 g]	2,2
Liquidity limit LL [%] (NF P 94-051)	28
Plastic limit PL [%] (NF P 94-051)	21
Plasticity Index PI [%] (NF P 94-051)	7
Unified Soil Classification System (USCS)	ML

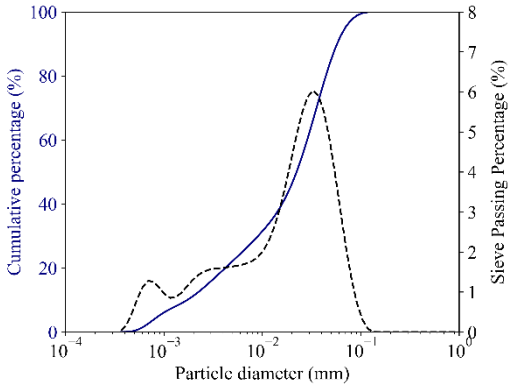

Figure 1: Particle size distribution.

2.2 Lime

The wet silt was stabilized with 1% lime. The quicklime content corresponds to free lime (or unbound), which is able to react chemically with the available water. The X-ray diffraction analysis conducted on lime highlights the purity of the product used with a majority of quicklime (89.6% of CaO) which was low in carbonate (0.4% of $CaCO_3$) and hydrate (7.1% of $Ca(OH)_2$). Its specific surface was measured at 6550 cm^2/g.

2.3 Cement

The 5% cement dosage is classic in linear projects. The low-carbon hydraulic binder chosen is based on a blast furnace slag with a composition similar to CEM III/A. It has a claimed composition of approximately 35% Portland cement clinker and 65% blast furnace slag (from spectrometry analysis: 48.2% CaO, 30.8 of SiO_2, 7.1 of Al_2O_3, 1.06 of Fe_2O_3, 4.56 of MgO, 1.34 of K_2O, 0.57 of Na_2O and 2.76 of SO_3 and RDX and TGA analysis: Quartz, Alite – C_3S, Belite - C_2S, Aluminate - C_3A, Brownmillerite – C_4AF, Calcite, Portlandite, Gypsum and Anhydrite). It is usually used to treat soils in place and in mixing stations. Its specific surface measured is 5120 cm^2/g.

2.4 Specimen preparation

Standard Proctor test (NF P94-093, 2014) was conducted to determine the Optimum Moisture Content (OMC) [%] corresponding to the maximum dry density [Mg/m^3] for a mixture of silt with 1% lime and

5% cement. The results of the test are presented in Figure 2 with the dry density as a function of the water content [%]. The Proctor curve is displayed with the saturation ratio (Sr [%]) curves which correspond to 100%, 90% and 80% pore water saturation. The maximum dry density measured (ρd = 1.75 Mg/m^3) corresponds to an OMC w = 17.5%.

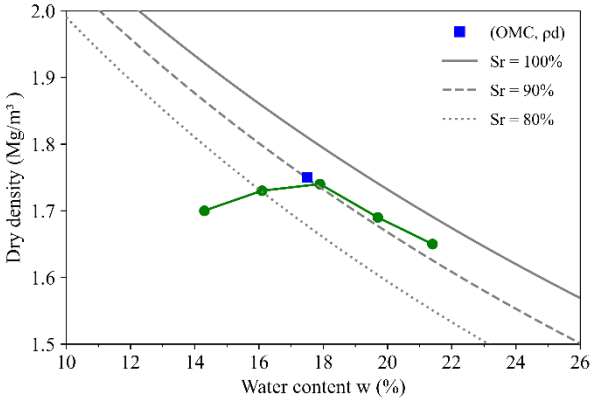

Figure 2: Proctors curve and saturation curves (Sr = 80%, 90%, 100%)

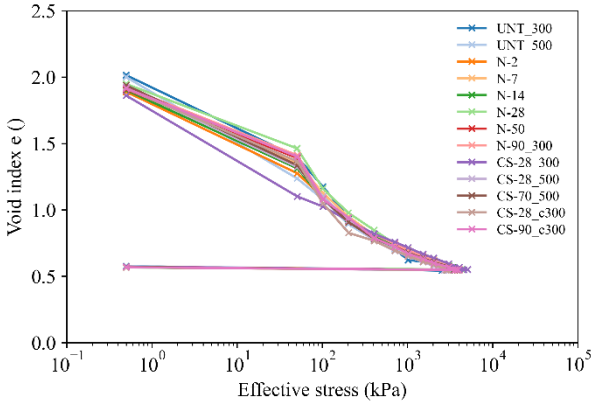

Figure 3: Compaction curves

In order to reproduce the treatment process used on site, the same sequencing was reproduced in the laboratory. First, the addition of lime caused the soil to flocculate. Then the cement was added, and the soil was mixed until it was homogeneous. The mixture was statically compacted (Serratrice, 2018): it was placed in a single layer in a greased steel tube with an internal diameter of 50 mm and a height of 100mm. The force was applied on both sides of the cylinder until 96% of optimal density was reached. Filter paper was placed at the top and bottom of the tube extremities.

Figure 3 presents compactions curves for each specimen with e, the void index, as a function of sigma, the axial stress [kPa]. The curves provided an estimate of the homogeneity of the specimens produced. The average void index of the 16 specimens was e = 0.577. The initial void index of the specimens must be the same in order to be able to compare results tests (Fahey et al., 2011).

2.5 Curing and testing conditions

The characteristics of the 16 tested specimens are listed in Table 2. The two untreated silt specimens are UNT_300 and UNT_500. They were respectively tested at isotropic stresses of 300 kPa and 500 kPa.

Following the standards, to ensure hydration reactions in the soil, stabilized soil specimens must be stored hermetically at a temperature of 20°C (Das et al., 2022; Lemaire et al., 2013). These conditions were respected in both types of curing compared in the study:

- Some specimens (N-2, N-7, N-14, N-28, N-50 and N-90) were hermetically protected and placed in an air-conditioned room at 20°C and atmospheric pressure (Patm).Those were maintained in this condition for a defined curing time (2, 7, 14, 28, 50 and 90 days) and a different specimen was used for each curing time test.
- Specimens subjected to curing stress (CS-28_300, CS-28_500 and CS-70_500), were directly placed in the RCA cell, in a neoprene membrane with damp filter paper at the extremities. Two specimens where placed in the RCA from 0 to 28 days under an isotropic curing stress of CS = 300 or 500 kPa (respectively CS-28_300 and CS-28_500) and one from 0 to 70 days at CS = 500 kPa (CS-70_500). For the CS-28_300 specimen, tests were carried out at 0, 1, 2, 3, 4, 7, 8, 9, 11, 14, 16, 18, 21, 23, 25 and 28 days. For CS-70_500, they were carried out at 0, 1, 2, 3, 6, 7, 8, 12, 14, 17, 20, 21, 23, 24, 28, 34, 35, 37, 42 45, 49, 52, 56, 59, 63, 66 and 69 days.
- A third type of curing condition was tested out to approximate the test protocols of previous authors working on curing stress. For this, the specimens were compacted and placed in a cell at CS = 300 kPa for 28 and 90 days (CS-28_c300 and CS-90_c300). The specimens were then removed from the cell and placed in the RCA cell (unloading and reloading) for testing at 300 kPa.

Table 2: Specimens curing and testing conditions.

Specimen	Test	Curing stress (kPa)	Curing time (days)	Testing pressure (kPa)	Tests per specimen
UNT_300	RCA untreated	Patm	-	300	1
UNT_500	RCA untreated	Patm	-	500	1
N-2	RCA 2 days	Patm	2	300 - 500	2
N-7	RCA 7 days	Patm	7	300 - 500	2
N-14	RCA 14 days	Patm	14	300 - 500	2
N-28	RCA 28 days	Patm	28	300 - 500	2
N-50	RCA 50 days	Patm	50	300 - 500	2
N-90	RCA 90 days	Patm	90	300 - 500	2
N-270	RCA 270 days	Patm	270	300 - 500	2

CS-28_300	RCA 28 days CS	300	28	300	16
CS-28_500	RCA 28 days CS	500	28	500	13
CS-70_500	RCA 70 days CS	500	70	500	29
CS-28_c300	RCA 28 days CS in cell	300	28	300	1
CS-90_c300	RCA 90 days CS in cell	300	90	300	1

**RCA: Resonant column apparatus use in torsional mode - UNT: Untreated - N: Normalized - CS: Curing stress – c: cell – Patm : Atmospheric pressure.*

3. Resonant column apparatus (RCA)

In torsion mode, the RCA test consists of exciting the top of the specimen by performing a torsional movement of a predetermined amplitude over a given frequency interval until the maximum amplitude of the response is reached. This maximum amplitude Amax [V] corresponds to the resonance frequency f_n [Hz] of the material under test. Shear wave velocity V_s [$m.s^{-1}$] (1) permits to calculate the shear modulus G [MPa] (2):

$$V_s = \frac{\omega_n L}{\beta} \quad (1)$$

$$G = \rho V_s^2 \quad (2)$$

Where ωn is the angular frequency [$rad \cdot s^{-1}$] corresponding to $\omega_n = 2\pi f_n$. The resonance frequency is the lowest frequency at which the torsion is 90° out of phase with the rotational displacement. L [m] is the length of the specimen and D its diameter [m]. The parameter β depends on the apparatus specificities. ρ is the specimen density [$g.cm^3$]. This test allows shear modulus measurements at strains between 3^{e-7} (rigid materials) and 2^{e-3} (softer materials). The distortion (ϒ) [] associated to the frequency peak is calculated with the following formula:

$$\Upsilon = \frac{4{,}596.A_{max}.D}{f_n.L} \quad (3)$$

A total of 74 tests were executed for this study. A test corresponded to a series of about 25 points performed in the range of amplitude between 0.005 V and 1 V. The tests were performed starting at the lowest amplitudes (0.005 V) up to the highest (1 V). All the present tests were conducted on unsaturated

specimens with drain open to the air, at testing pressure of 300 kPa or 500 kPa. The G modulus measured at the smaller amplitudes (0.005 V) with an RCA was designated Gmax.

4. Results and discussions

4.1 Degradations curves

As mentioned previously, the aim of the tests was to highlight the effect of curing stress on the kinetic mechanical properties' evolution. The RCA device provides resonance peaks at each amplitude step imposed. The previous equations give shear modulus G [MPa] degradation curves as a function of the distortion for the different specimens and each curing condition (Figures 4 to 7, graphs (a)). The normalized decreased curves (G/Gmax) as a function of the shear strain are also presented (Figure 4 to 7, graphs (b)).

Before improving the soil, tests were carried out on untreated compacted soil specimens (blue crosses in Figures 4 to 7) with the same test conditions (unsaturated specimens, open drainage to air). The testing pressures used were 300 and 500 kPa (specimens UNT_300 and UNT_500, respectively). At 300 kPa, the untreated silt specimen has a Gmax of 135 MPa which corresponds to a shear deformation of 5^{e-6}. At 500 kPa, the untreated silt specimen has a Gmax of 175 MPa, which corresponds to a shear deformation of 5^{e-6}. By comparison, the specimens of stabilized soil are located on much smaller deformations which decelerate according to the curing time as the specimen stiffens. As summarized in Table 2, a different specimen was used for each curing time to study the mechanical properties after curing at atmospheric pressure. The results are illustrated in Figures 4 and 5.

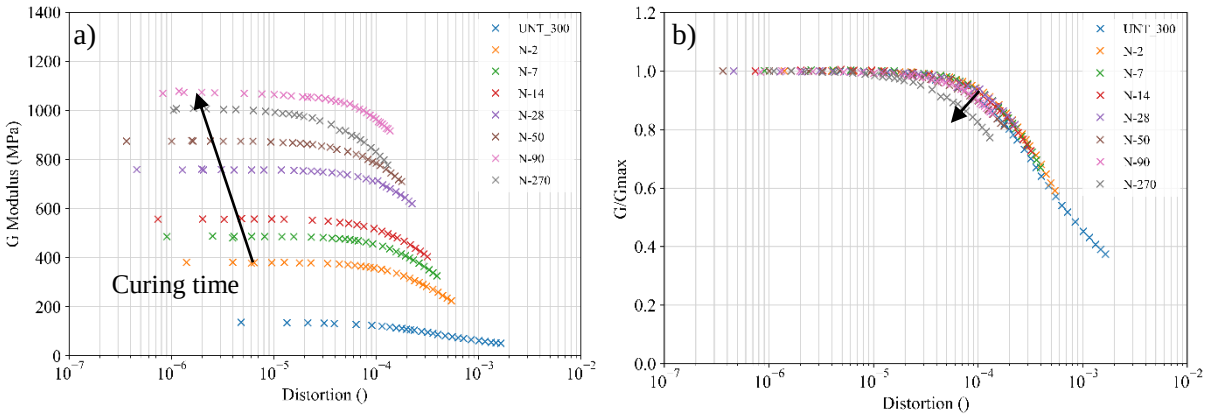

Figure 4 : RCA tests results for atmospheric pressure curing condition (testing pressure of 300 kPa). (a) Degradation curves: G modulus as a function of shear strain (b) G/Gmax curves as a function of shear strain

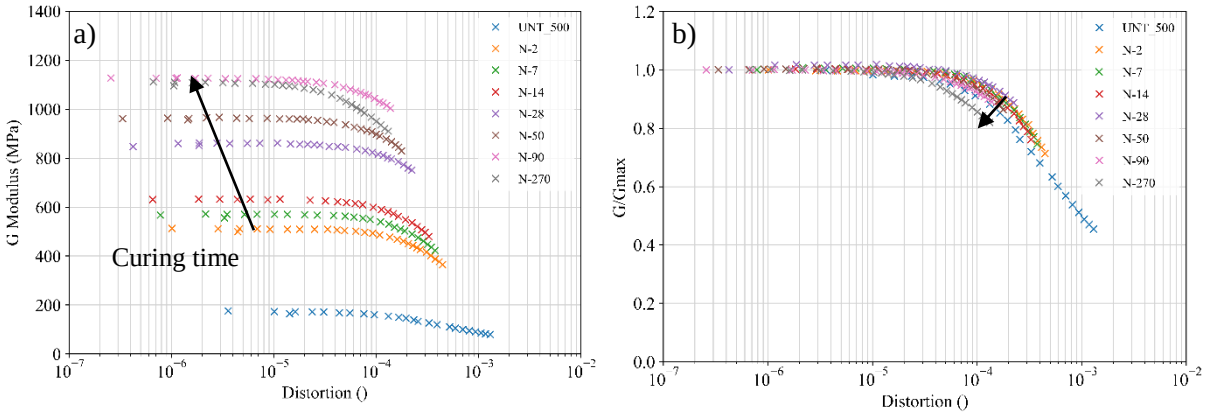

Figure 5: RCA tests results for atmospheric pressure curing condition (testing pressure of 500 kPa). (a) Degradation curves: G modulus as a function of shear strain (b) G/Gmax curves as a function of shear strain.

To investigate the influence of curing stress, 3 specimens were realized (testing pressure of 300 kPa: CS-28_300, testing pressure of 500 kPa: CS-28_500, CS-70_500, see Table 2). However, since the results of the CS-28_500 test were identical to the first 28 days of the CS-70_500 test, they are not presented. The evolution of the shear moduli from 0 to 28 days at 300 kPa curing stress is reported in Figure 6. At 500 kPa, the G modulus evolution was measured up to 70 days (see Figure 7). In the legends to Figure 6 and Figure 7, the day of the cure on which the test was carried out is indicated by "1d" (for the first day of curing, for example). In these figures, the arrows show the evolution of the degradation curves from the first day to the last day curing.

For each curing condition, the lowest G moduli are observed for the specimens with the youngest age (see Figures 4 to 7). At higher cure times, the curves have minimal G moduli at lower displacements because the RCA can only measure resonance peaks up to an amplitude of 1 V.

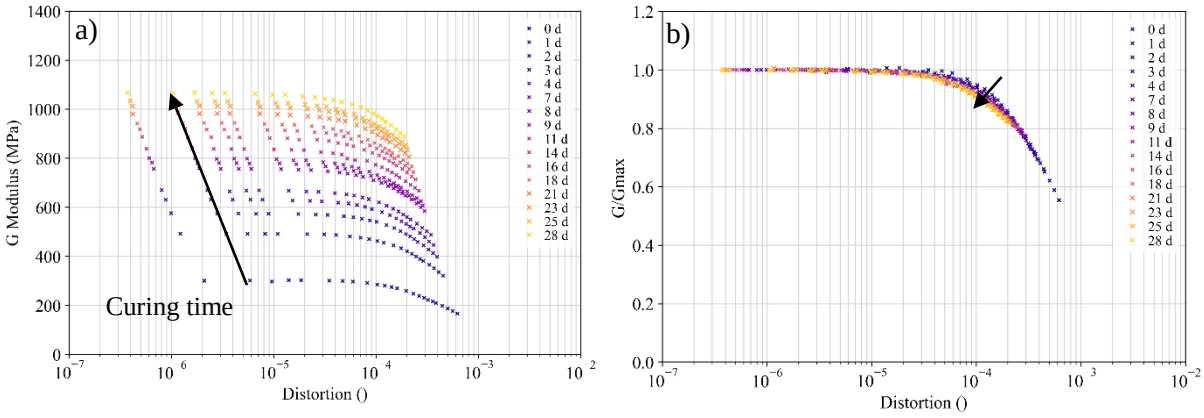

Figure 6: Specimen CS-28_300 cured with a curing stress of 300 kPa for 28 days (testing pressure of 300 kPa).
(a) Degradation curves: G modulus as a function of shear strain
(b) G/Gmax curves as a function of shear strain.

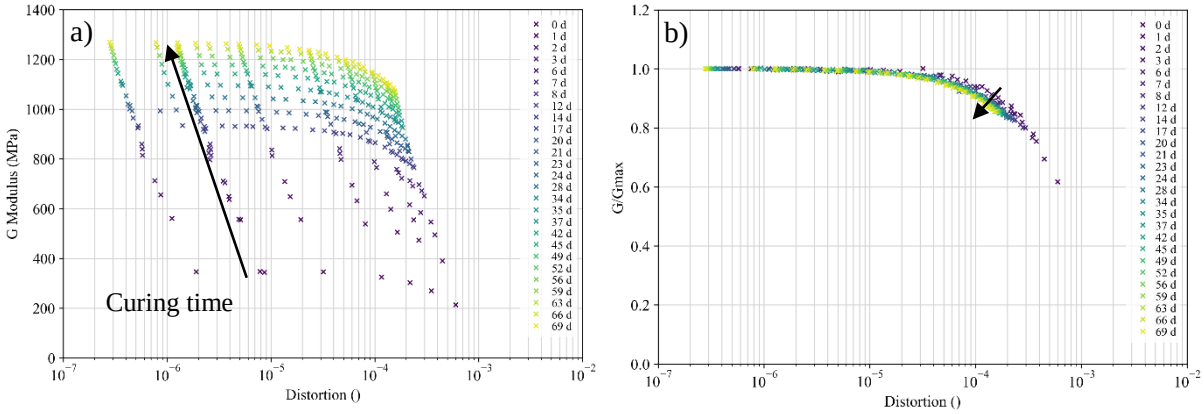

Figure 7: Specimen CS-70_500 cured with an isotropic stress of 500 kPa for 70 days (testing pressure of 500 kPa).
(a) Degradation curves: G modulus as a function of shear strain,
(b) G/Gmax curves as a function of shear strain.

Globally, the mechanical evolution within the specimen as a function of curing time is visible at several levels: the evolution of the shape of the curves, the increase in Gmax as a function of time, and the shift of the curve towards smaller deformations.

After a curing period of 90 days without any curing stress, tests performed at testing pressure of 300 kPa provide a G modulus value of 1073 MPa for the specimen. In contrast, with curing stresses, the G modulus value reaches 1067 MPa after only 28 days. Therefore, the specimen CS-70_500, after 41 days

with a curing stress of 500 kPa, reaches the same modulus as the specimen N-90 after 90 days of curing without stress (CS-70_500, Gmax = 1137 MPa ; N-90, Gmax = 1127 MPa). The influence of the testing pressure seems to be more important for the tests carried out after a cure without curing stress. For example, after a curing time of 90 days without curing stress, there is a difference of 55 MPa between the test performed at 300 kPa and 500 kPa. By contrast, for the tests on specimens subjected to curing stress, the difference in testing pressure between 300 and 500 kPa does not generate any difference between the moduli obtained.

Concerning the G/Gmax evolution versus distortion, one notices that the shape of the curves for the same curing conditions is similar but shifts according to the black arrow added to the graphs (Figures 6 (b) and 7 (b)).

4.2 Effect of curing stress on the evolution of Gmax as a function of time

Previous results can provide the evolution of Gmax [MPa] as a function of curing time [days] as illustrated by Figure 8 (see Appendix for all Gmax values for each specimen). The results show two different hydration kinetics. The first one corresponds to specimens cured with a curing stress of 300 kPa (CS-28_300, purple dots) and a curing stress of 500 kPa (CS-70_500, green dots). The second one corresponds to specimens cured without stress and tested at different curing times with the RCA at a testing pressure of 300 kPa (purple cross) or 500 kPa (green cross). For this last curing condition, each cross represents a unique specimen, in contrast to CS-28_300 and CS-70_500 curves, for which each point corresponds to the same specimen. The triangle and the blue star represent the Gmax of a specimen that has been cured in confining cell and subjected to a cycle of loading/unloading/reloading (for the test in the RCA) at 300 kPa after a curing time of 28 days (CS-28_c300) and 90 days (CS-90_c300).

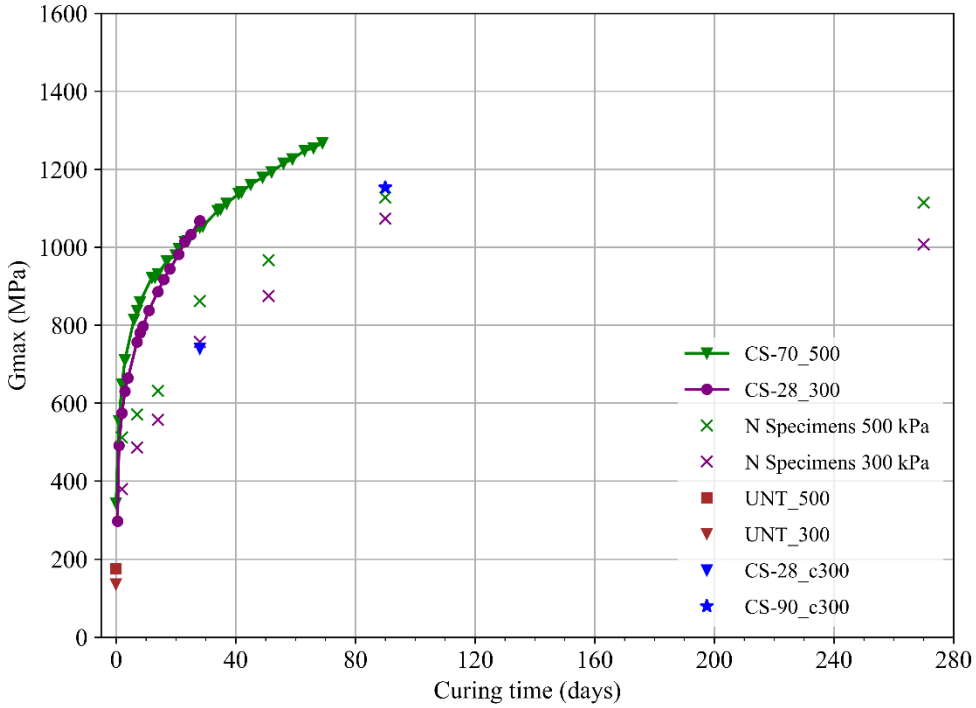

Figure 8 : Evolution of shear modulus Gmax as a function of time for each curing condition.

Table 3: Percentage increase in Gmax modulus as a function of time and curing conditions.

Specimen	Gmax after 0* day (MPa)	Gmax after 2 days (MPa)	Gmax after 28 days (MPa)	Gain from 0 to 2 days (%)	Gain from 2 to 28 days (%)	Gain from 0 to 28 days (%)
N- (300)	-	380	757	-	99	-
CS-28_300	302	575	1068	90	86	254
N- (500)	-	512	861	-	68	-
CS-70_500	352	655	1053	89	61	203

*Around 5 hours after compaction.

Table 3 presents the analysis of the percentage increase in G modulus for different curing conditions shown in Figure 8. For specimens without curing stress, from 2 to 28 days, Gmax increases by 99% for 300 kPa testing pressure and by 68% for 500 kPa. When the curing stress is 300 kPa (CS-28_300), from 0 to 28 days, Gmax increases by 254% (from 302 MPa at 0 days of curing to up to 1070 after 28 days). When the curing stress is 500 kPa, Gmax increases by 203% from 0 to 28 days.

The percentage increase between 2 and 28 days for the two types of curing is almost identical (for tests at 300 kPa: 99% and 86%, and for tests at 500 kPa: 68%, and 161%). On the whole, the kinetics of the modulus increase is very high during the first 2 days and then grows more slowly until it reaches a

threshold. Indeed the Table 3 show that the shear modulus G increases more between 0 and 2 days of curing than between 2 and 28 days of curing.

Previous studies have focused on the increase of the Gmax G and its link with the chemical reactions of hydration caused by the addition of hydraulic binders (Di Sante et al., 2022). The kinetics observed in Figure 8 can be explained by isothermal calorimetry tests carried out on soil mixtures with lime and cement (Bouras, 2020). These show two peaks in heat release after mixing: a peak associated with lime in the first two hours and over the following 12 hours, heat associated with cement. Pozzolanic reactions continue to develop over the long term, after which the quantity of non-hydrated anhydrous decreases and reactions slow down (Bell, 1996). This is illustrated by Figure 8, which show an increase in Gmax up to 90 days, followed by stabilization of the modulus up to 270 days. These results reinforce the idea that after 90 days most of the hydration reactions had been achieved (LCPC/SETRA, 2000). For specimens subjected to curing stress, the study does not go beyond 70 days, but one cannot rule out the hypothesis that a plateau is reached after 90 days as well.

As noted earlier, between specimens with the same curing condition, the influence of confining pressure is not noticeable for specimens in curing stress. Indeed, at 28 days the measured modulus Gmax of the soil is the same under a pressure of 300 kPa and 500 kPa. It would be interesting to carry out these tests with greater number of curing stresses values. This could eventually lead to determine the minimum curing stress necessary to impact the kinetics of the material mechanical properties improvement or the presence of a pressure threshold beyond which the Gmax remains stable.

During the time that specimens are held under confining pressure, axial displacement shows a slight settlement that occurs on the first day of curing but after no consolidation-related settlement is measured. These measurements reveal that the increase in G modulus as a function of time is not a function of a mechanical change in the soil but rather the result of chemical reactions with the lime and cement. Indeed, the kinetics of module growth with confining pressure seem to be explained by faster and better hydration of the anhydrous phases of cement and lime in the soil. Some authors explain this kinetic by a macroscopically unmeasurable rapprochement of the soil aggregates induced by the curing stress that increases the contact area between them without causing a significant densification of the material (Cui

& Fall, 2016). Enhancing contact between soil grains via curing stress would increase the contact between the cement shells, resulting in stronger cementitious bonds and thus solidifying the structure as a whole.

4.3 A power law to predict Gmax as a function of time

One of the aim of the study is to predict Gmax as a function of time up to 90 days. Indeed, as observed previously (Figure 8), this curing time seems to correspond to the time required to attract the stabilized properties of the stabilized silt. The experimental results showed that knowing the Gmax at 90 days gave an indication of the Gmax over the long term (at least up to 270 days). This applies in conditions where the material is not mechanically or chemically degraded. Some authors have tried to predict the time-dependent behavior of these soils using tests carried out in the first days after the addition of binders. For example, a power law that predicts the behavior of a lime-treated clay soil at 28 days of curing based on data from the first 2 days was proposed by (Toohey & Mooney, 2012). They suggested the following equation:

$$G_{max}(t) = G_{\max t1}\left(\frac{t}{t_1}\right)^{\alpha} \quad (4)$$

Where Gmax(t) [MPa] represented the maximum shear modulus value at a specific time t [day]. The growth rate of the Gmax modulus compared to $G_{max\ t1}$ (Gmax modulus at day 1) was represented by the parameter α. This model was based on the fact that most of the growth of the modulus takes place during the first two days of curing.

In accordance with the experimental results, it is possible to propose a law based on Equation (4) and beyond 28 days:

$$0 \le t \le 90\ days \quad G_{\max}(t) = G_{\max t1}\left(\frac{t}{t1}\right)^{\alpha(Cp,CS\ or\ CN)} \quad (5)$$

$$t \ge 90\ days \quad G_{\max}(t) = G_{max}(t90)$$

Where the α parameter depends on the confining pressure to which the specimen is subjected during curing (CS or CN) and during the RCA test (Cp), and Gmax(t90) is the maximum shear modulus Gmax after 90 days of curing.

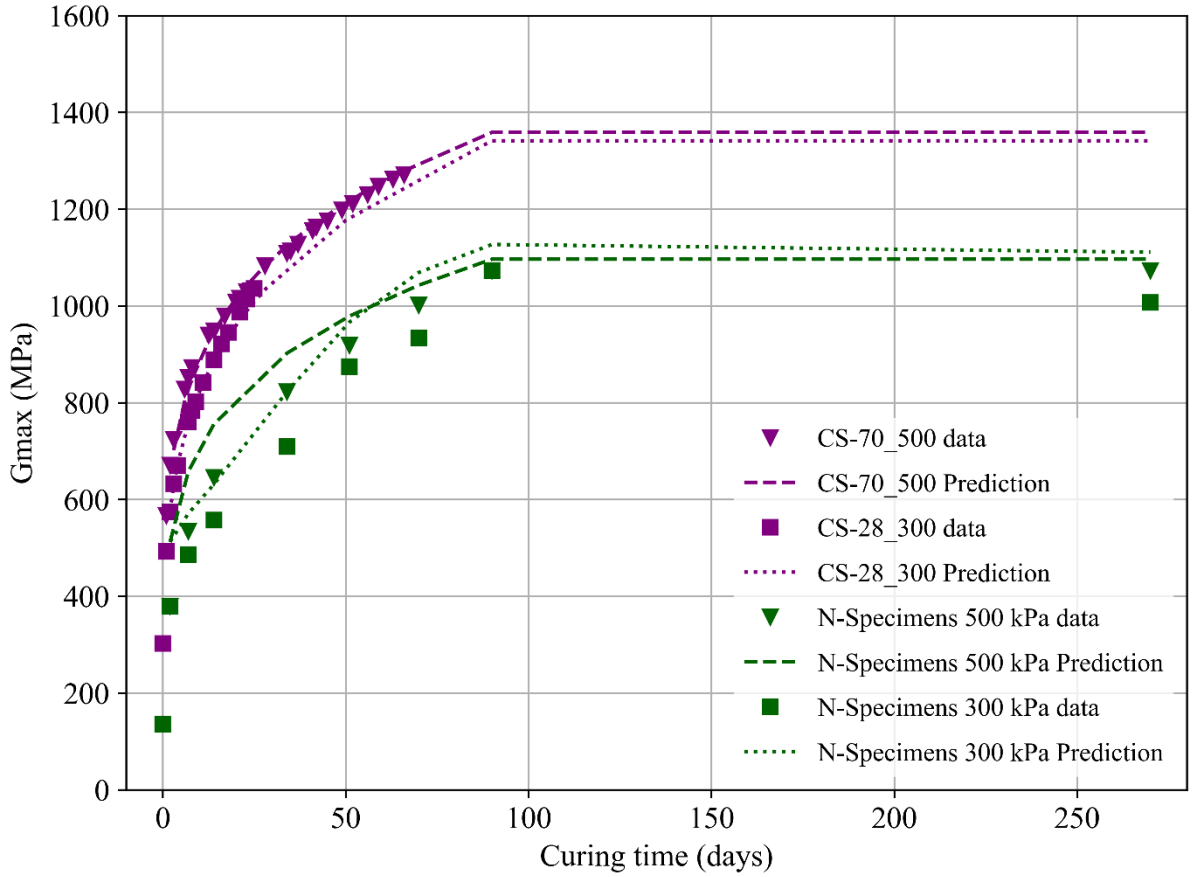

Figure 9: Prediction of Gmax as a function of time using equation 5.

Table 4: α parameters and R^2 obtained for the regression of Gmax against time with equation 5.

	Specimens with curing stress (CS)			**Specimens without curing stress (N-)**	
	CS-28_300	CS-28_500	CS-70_500	Tests at 300 kPa	Tests at 500 kPa
α	0.23	0.19	0.19	0.27	0.21
R^2	0.999	0.997	0.997	0.981	0.943

The results of this power law are shown in Figure 9 where the dots correspond to the experimental measurements and the dashed curves to the law predictions (Equation 5). The curves of the tests on specimens without curing stress are plotted in green. The curves of the specimens subjected to curing stress (CS-28_300, CS-28_500 and CS-70_500) are shown in blue and purple.

The alpha parameter (α) optimized for each curve according to the experimental data and the difference (R^2) between these curves and the measured data are shown in Table 4. In the Mooney and Toohey's study which sets out the previous empirical law (Equation 4), several types of soils with varying degrees of clay content were treated and the parameter α was characteristic of each soil type. The parameter α in Equation 5, which is a function of the confining pressure during curing and testing, decreases as these pressures decrease. The Figure 10 shows that the gradient is the same between the parameter α of specimens in normalized curing (N) as between the α of specimens in curing stress. An equation (6) is proposed to calculate α as a function of the confining pressure during curing (CS) and during the test (Cp):

$$For\ N\ specimens : \propto = 2{,}5.10^{-4}Cp + 3{,}55.10^{-1}$$

$$For\ CS\ specimens : \propto = 2{,}5.10^{-4}Cp + 3{,}05.10^{-1} \quad (6)$$

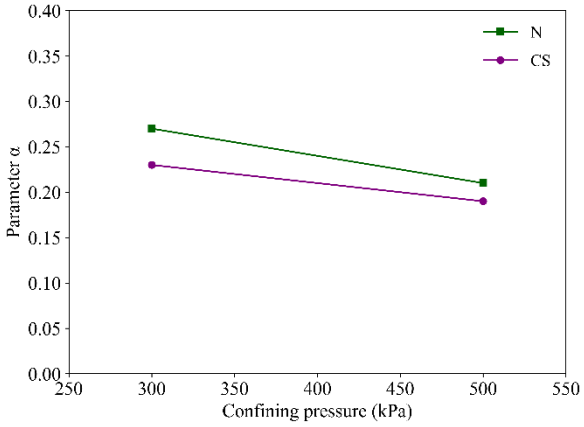

Figure 10 : Evolution of parameter as function of the confining pressure.

The high R^2 values (> 0.94) in Table 4 demonstrate that the power law effectively models the relationship between Gmax and curing time. Particularly noteworthy is the remarkably high R^2 value of 0.997 obtained for the CS-70 specimen, based on a robust dataset of 29 measurements. This result strongly supports the power law's ability to accurately model the Gmax-curing time relationship. The consistency of parameter values across specimens indicates homogeneous material properties and repeatable test results. However, tests without curing stress exhibit slightly higher variation, likely due to the use of different specimens at each time point. The model's robustness was verified by using Gmax at different reference times (7, 14, or 28 days). These variations in the starting Gmax value (Gmax_t1) did not

significantly impact prediction accuracy, as evidenced by consistent α values and R^2. Therefore, this model allows for long-term prediction of Gmax at 90 days (and beyond) using just 2 days (or more) of experimental data. For a given soil and treatment, the model can predict Gmax at 28 days under curing stress using the Gmax at 90 days under normal curing conditions, and vice versa.

While the power law model demonstrates promising results, it is important to acknowledge its limitations and explore potential avenues for further research. The model's performance might be affected by specific curing conditions or variations in soil properties like initial moisture content or binder dosage. Future studies could investigate the model's applicability under a wider range of conditions to assess its robustness.

Additionally, the model's current focus is on predicting Gmax at 90 days. Extending the prediction capability beyond 270 days would be valuable for long-term assessments of stabilized soil behavior. Furthermore, incorporating additional data points beyond the first two days could potentially refine the model's accuracy. In terms of practical applications, predicting long-term Gmax has significant implications for geotechnical engineering. It could aid in optimizing construction schedules by providing more accurate estimates of soil strength over time. Moreover, it could facilitate the assessment of long-term stability for structures built on stabilized soils, enhancing safety and reducing the risk of infrastructure failures.

4.4 Proposal to simplify the experimental protocol

In order to predict in the laboratory the mechanical properties of a stabilized soil when it is placed at a certain depth of a backfill while it is being cured, but without having to place the specimen in a RCA throughout the curing period, an experiment was carried out. The specimens were placed in a cell with a curing stress, then unloaded and reloaded in the resonant column cell. Finally, a torsional test was performed a few hours later. Two tests were conducted after 28 days and 90 days of curing time (respectively on specimens CS-28_c300 and CS-90_c300). Indeed, a minimum of 28 days of curing stress is recommended to stabilize the cementitious bonds between specimen particles. (Fahey et al., 2011) has shown that 7 days with a curing stress of 800 kPa was not sufficient to provide a soil cement

mix with sufficiently strong cementitious bridges to withstand an unloading until 0 kPa. During the 7 days of curing stress shear modulus raised and it decreased after unloading.

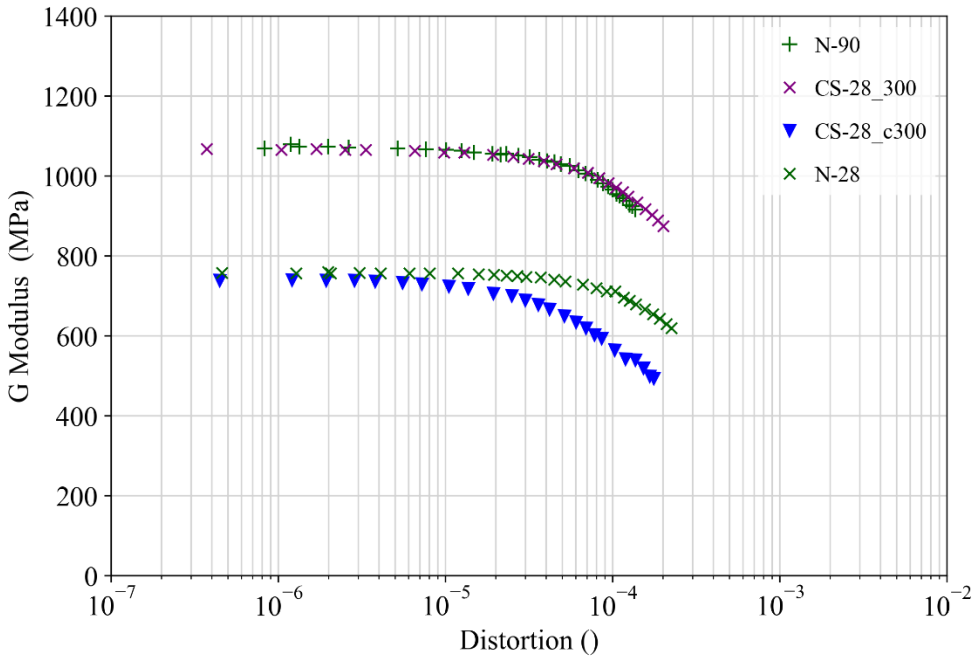

Figure 11: Impact of an unloading cycle on the curing stress specimen after curing for 28 days in a cell and tested in the RCA (N-28, CS-28_300 and CS-28_c300).

Figure 11 shows G modulus as a function of distortion and compares the results of a test with curing stress (CS-28_300, in yellow), without curing stress (N-28, in purple) and the unloading test (CS-28_c300, in green). Globally, the shape of the curves is identical for these three different curing conditions. However, after a curing time of 28 days (CS-28_c300), the Gmax value obtained is 862 MPa. In comparison, the specimen that was cured in the resonant column cell without being moved (CS-28_300) has a Gmax of 1068 MPa for the same curing time. The specimen without curing stress (N-28) has a Gmax of 709 MPa after 28 days. This test confirms that 28 days of curing stress is not sufficient to produce cementitious bonds that are strong enough to resist unloading. However, the modulus is much higher than that of the specimen without curing stress, which shows an improvement of the hydration process with curing stress.

As can be seen in Figure 9, even after 90 days of curing time (CS-90_c300), the cementitious bridges formed between the shells surrounding the natural soil aggregates are not strong enough to resist unloading. Indeed, the G modulus obtained are practically identical to those observed for a curing time

without curing stress. In order to explain these differences, previous authors conducted a number of tests to compare the amount of hydrates between a specimen with or without curing stress. Thermogravimetric analysis (TGA) and X-ray diffraction (XRD) tests are performed to monitor the evolution of hydrates and anhydrous phases within cementitious materials. Performed on CPB or soil mixing specimens, these tests show a faster and greater amount of consumed cementitious phases and hydrates in the specimens that had curing stress (Chen et al., 2021; Zhao et al., 2021). Very high-pressure (100 MPa – 40 MPa) favors the dissolution of C3S (visible by the increase in conductivity) so that Portlandite and CSH are formed earlier (Bresson et al., 2002). However, in stabilized soils, it is quite difficult to distinguish hydrated phases because of the amount of treatment (<10%) and because the hydrated phases formed are often not sufficiently crystallized (Lemaire et al., 2013). Another aspect that can be studied using SEM (scanning electron microscope) observations is the difference in density of hydrate matrices with or without curing stress. In the first configuration, hydrates have a denser matrix and fewer visible macropores, and cracks are observed (Zhao et al., 2021).

To conclude, confining the specimen in a 28 or 90 day cell and placing it in the resonant column for a torsion test leads to a degradation of the Gmax, and therefore a poor representability of the Gmax of the specimen if it had not been unloaded. It is recommended to conduct a test after the specimen has been cured for 1 or 2 days and then use equation (5) to predict its Gmax over the long term.

5. Conclusion

In the context of a linear infrastructure project, the present study experimentally investigates the shear modulus degradation curves of stabilized silt specimens with different curing conditions in laboratory with a resonant column apparatus. The specimens of soil stabilized with 1% lime and 5% cement were maintained under curing conditions of 20°C and atmospheric pressure or 20°C and isotropic confining pressure around the specimen. The tests were conducted with curing and testing pressures of 300 and 500 kPa, which represent the presence of soil in a high embankment.

The main conclusions are as follows:

(1) The paper focuses on the shear modulus degradation curves as a function of curing time. These curves show the stiffening of the natural soil by the addition of lime, a hydraulic binder, and by compaction.

(2) The resonant column makes it possible to combine the curing and testing phases and thus to represent the evolution of the treated soil within an embankment as a function of its curing time. Indeed, this enables continuous monitoring from the first few hours up to durations not reached in the literature (70 days).

(3) A power law has been proposed which allows Gmax to be predicted over the long term (270 days) using the Gmax after 1 or 2 days of curing (for both normalized and curing stress conditions). The α parameter of the law depends on the cure and test pressure.

(4) Even after 90 days curing with stresses, the cementitious bridges formed between the shells surrounding the natural soil aggregates are not strong enough to resist unloading.

(5) Further work is underway to investigate the microstructure and chemical composition inherent to these mechanical tests. Indeed, an important question for future studies is to understand the influence of curing stress on the mechanical properties of binder and lime-treated silt.

6. Acknowledgments

The tests were made possible thanks to the work of Laurent Batilliot (GeoCoD, Cerema). The PhD project is funded by EGIS STRUCTURES ET ENVIRONNEMENT and Centrale Nantes. We also wish to thank the Seine Nord Europe Canal Company.

7. References

Åhnberg, H. (2007). On yield stresses and the influence of curing stresses on stress paths and strength measured in triaxial testing of stabilized soils. *Canadian Geotechnical Journal*, *44*(1), 54-66. https://doi.org/10.1139/t06-096

ASTM. (2020). D2488 : Practice for Classification of Soils for Engineering Purposes (Unified Soil Classification System). *ASTM International, West Conshohocken, PA, USA*. https://doi.org/10.1520/D2487-17E01

ASTM. (2021). D4015—21 : Test Methods for Modulus and Damping of Soils by Fixed-Base Resonant Column Devices. *ASTM International, West Conshohocken, PA, USA*. https://doi.org/10.1520/D4015-21

Bell, F. G. (1996). Lime stabilization of clay minerals and soils. *Engineering Geology*, *42*(4), 223-237. https://doi.org/10.1016/0013-7952(96)00028-2

Bouras, F. (2020). *Le traitement de sols argileux : Approches physico-chimique et géotechnique* [Doctoral dissertation]. Université d'Orléans.

Bresson, B., Méducin, F., Zanni, H., & Noïk, C. (2002). Hydration of Tricalcium Silicate (C3S) at High Temperature and High Pressure. *Journal of Materials Science - J MATER SCI*, *37*, 5355-5365. https://doi.org/10.1023/A:1021093528888

Chae, Y. S., Au, W. C., & Chiang, Y. C. (1981). *Determination of Dynamic Shear Modulus of Soils from Static Strength*. 7.

Chen, S., Wu, A., Wang, Y., & Wang, W. (2021). Coupled effects of curing stress and curing temperature on mechanical and physical properties of cemented paste backfill. *Construction and Building Materials*, *273*, 121746. https://doi.org/10.1016/j.conbuildmat.2020.121746

Chepkoit, K. K., & Aggour, M. S. (1996). *Dynamic properties of untreated and treated cohesive soils*. 8.

Chiang, Y., & Chae, Y. (1972). Dynamic properties of cement-treated soils. *Highway Research Record*. https://www.semanticscholar.org/paper/DYNAMIC-PROPERTIES-OF-CEMENT-TREATED-SOILS-Chiang-Chae/48833895700b0a37b0b995a75f34a7affc71515a

Consoli, N. C., Rotta, G. V., & Prietto, P. D. M. (2000). Influence of curing under stress on the triaxial response of cemented soils. *Géotechnique*, *50*(1), 99-105. https://doi.org/10.1680/geot.2000.50.1.99

Cui, L., & Fall, M. (2016). Mechanical and thermal properties of cemented tailings materials at early ages : Influence of initial temperature, curing stress and drainage conditions. *Construction and Building Materials*, *125*, 553-563. https://doi.org/10.1016/j.conbuildmat.2016.08.080

Dalla Rosa, F., Consoli, N. C., & Baudet, B. A. (2008). An experimental investigation of the behaviour of artificially cemented soil cured under stress. *Géotechnique*, *58*(8), 675-679. https://doi.org/10.1680/geot.2008.58.8.675

Das, G., Razakamanantsoa, A., Herrier, G., & Deneele, D. (2022). Influence of pore fluid-soil structure interactions on compacted lime-treated silty soil. *Engineering Geology*, *296*, 106496. https://doi.org/10.1016/j.enggeo.2021.106496

Di Sante, M., Bernardo, D., Bellezza, I., Fratalocchi, E., & Mazzieri, F. (2022). Linking small-strain stiffness to development of chemical reactions in lime-treated soils. *Transportation Geotechnics*, *34*, 100742. https://doi.org/10.1016/j.trgeo.2022.100742

Fahey, M., Helinski, M., & Fourie, A. (2011). Development of Specimen Curing Procedures that Account for the Influence of Effective Stress During Curing on the Strength of Cemented Mine Backfill. *Geotechnical and Geological Engineering*, *29*(5), 709-723. https://doi.org/10.1007/s10706-011-9412-2

Filipe Veloso Marques, S., Cesar Consoli, N., & Festugato, L. (2019). Effects of curing stress on the stiffness of a cement-mixed sand. *E3S Web of Conferences*, *92*, 04006. https://doi.org/10.1051/e3sconf/20199204006

He, X., Chen, Y., Wan, Y., Liu, L., & Xue, Q. (2020). Effect of Curing Stress on Compression Behavior of Cement-Treated Dredged Sediment. *International Journal of Geomechanics*, *20*(11), 04020204. https://doi.org/10.1061/(ASCE)GM.1943-5622.0001857

ISO. (2020). *Particle size analysis—Laser diffraction methods*. https://www.iso.org/fr/standard/69111.html

Lang, L., Li, F., & Chen, B. (2020). Small-strain dynamic properties of silty clay stabilized by cement and fly ash. *Construction and Building Materials*, *237*, 117646. https://doi.org/10.1016/j.conbuildmat.2019.117646

LCPC/SETRA. (2000). *Traitement des sols à la chaux et/ou aux liants hydrauliques. Application à la réalisation des remblais et des couches de forme. Guide de Traitement des sols (GTS)* (Réf. D9924). LCPC.

Lemaire, K., Deneele, D., Bonnet, S., & Legret, M. (2013). Effects of lime and cement treatment on the physicochemical, microstructural and mechanical characteristics of a plastic silt. *Engineering Geology*, *166*, 255-261. https://doi.org/10.1016/j.enggeo.2013.09.012

Liu, C., & Starcher, R. D. (2013). Effects of Curing Conditions on Unconfined Compressive Strength of Cement- and Cement-Fiber-Improved Soft Soils. *Journal of Materials in Civil Engineering*, *25*(8), 1134-1141. https://doi.org/10.1061/(ASCE)MT.1943-5533.0000575

Makki-Szymkiewicz, L., Hibouche, A., Taibi, S., Herrier, G., Lesueur, D., & Fleureau, J.-M. (2015). Evolution of the properties of lime-treated silty soil in a small experimental embankment. *Engineering Geology*, *191*, 8-22. https://doi.org/10.1016/j.enggeo.2015.03.008

NF P94-093. (2014). *Sols : Reconnaissance et essais—Détermination des références de compactage d'un matériau—Essai Proctor Normal—Essai Proctor modifié* (Normes nationales et documents normatifs nationaux). https://www.boutique.afnor.org/fr-fr/norme/nf-p94093/sols-reconnaissance-et-essais-determination-des-references-de-compactage-du/fa185491/43924

Sariosseiri, F., & Muhunthan, B. (2009). Effect of cement treatment on geotechnical properties of some Washington State soils. *Engineering geology*, *104*(1-2), 119-125.

Serratrice, J.-F. (2018). Apport expérimental de la méthode de compactage statique des sols au laboratoire. *Revue Française de Géotechnique*, *156*, 1. https://doi.org/10.1051/geotech/2019001

Suzuki, M., Fujimoto, T., & Taguchi, T. (2014). Peak and residual strength characteristics of cement-treated soil cured under different consolidation conditions. *Soils and Foundations*, *54*(4), 687-698. https://doi.org/10.1016/j.sandf.2014.06.023

Taher, A., Rabb, Z., KUWANO, J., Deng, J., & BOON, T. (2011). Effect of Curing Stress and Period on the Mechanical Properties of Cement-Mixed Sand. *Soils and Foundations*, *51*, 651-661. https://doi.org/10.3208/sandf.51.651

Toohey, N. M., & Mooney, M. A. (2012). Seismic modulus growth of lime-stabilised soil during curing. *Géotechnique*, *62*(2), 161-170. https://doi.org/10.1680/geot.9.P.122

Tsai, P. H., & Ni, S. H. (2011). A Study on Dynamic Properties of Cement-Stabilized Soils. *Advanced Materials Research*, *243-249*, 2050-2054. https://doi.org/10.4028/www.scientific.net/AMR.243-249.2050

Wild, S., Kinuthia, J. M., Jones, G. I., & Higgins, D. D. (1998). Effects of partial substitution of lime with ground granulated blast furnace slag (GGBS) on the strength properties of lime-stabilised sulphate-bearing clay soils. *Engineering geology*, *51*(1), 37-53.

Yaghoubi, M., Arulrajah, A., Miri Disfani, M., Horpibulsuk, S., & Leong, M. (2020). Compressibility and strength development of geopolymer stabilized columns cured under stress. *Soils and Foundations*, *60*(5), 1241-1250. https://doi.org/10.1016/j.sandf.2020.07.005

Zhang, R.-J., Zheng, J., & Bian, X. (2017). Experimental investigation on effect of curing stress on the strength of cement-stabilized clay at high water content. *Acta Geotechnica*, *12*, 1-16. https://doi.org/10.1007/s11440-016-0511-3

Zhao, Y., Taheri, A., Karakus, M., Deng, A., & Guo, L. (2021). The Effect of Curing under Applied Stress on the Mechanical Performance of Cement Paste Backfill. *Minerals*, *11*(10), 1107. https://doi.org/10.3390/min11101107

Zhu, F., Clark, J. I., & Paulin, M. J. (1995). Factors affecting at-rest lateral stress in artificially cemented sands. *Canadian Geotechnical Journal*, *32*(2), 195-203. https://doi.org/10.1139/t95-023

Appendix

Specimens with normalized curing period

Specimen	Test pressure (kPa)	Gmax Modulus (MPa)	Gmin Modulus (MPa)
UNT_300	300	136	51
N-2	300	380	224
N-7	300	487	326
N-14	300	559	404
N-28	300	761	620
N-50	300	878	710
N-90	300	1073	916
N-270	300	1007	778
UNT_500	500	175	80
N-2	500	512	365
N-7	500	571	423
N-14	500	632	480
N-28	500	861	751
N-50	500	966	830
N-90	500	1128	1003
N-270	500	1112	909

CS-28_300

Curing time (days)	Gmax Modulus (MPa)	Gmin Modulus (MPa)
0	302	158

1	492	307
2	575	384
3	632	434
4	669	474
7	758	572
8	783	594
9	800	613
11	840	650
14	887	702
16	919	730
18	944	755
21	986	796
23	1016	823
25	1034	843
28	1068	875

C-**28_c300**

Curing time (days)	Gmax Modulus (MPa)	Gmin Modulus (MPa)
28	740	493

C-**90_c300**

Curing time (days)	Gmax Modulus (MPa)	Gmin Modulus (MPa)
0	1152	932

CS-28_500

Curing time (days)	Gmax Modulus (MPa)	Gmin Modulus (MPa)
0	342	219
1	542	386
2	625	461
3	672	513
4	709	549
7	786	638
9	826	675

14	910	768
18	950	807
22	982	840
24	1011	858
25	1013	858
28	1042	881

520

521 **CS-70_500**

Curing time (days)	Gmax Modulus (MPa)	Gmin Modulus (MPa)
0	347	-
1	560	389
2	655	494
3	712	546
6	815	652
7	839	672
8	859	696
12	924	765
14	934	770
17	964	799
20	993	829
21	1000	833
23	1014	850
24	1020	856
28	1053	892
34	1096	925
35	1102	946
37	1112	953
42	1147	986
45	1161	988
49	1183	1031
52	1196	1021
56	1215	1059

59	1232	1055
63	1248	1089
66	1256	1073
69	1269	1100

522

523